Simulation of the Seasonal Cycle of the Tropical Pacific Ocean

S. G. H. PHILANDER, W. J. HURLIN AND A. D. SEIGEL*

Geophysical Fluid Dynamics Laboratory/NOAA, Princeton University, Princeton, NJ 08542

(Manuscript received 15 December 1986, in final form 22 May 1987)

ABSTRACT

In a general circulation model of the tropical Pacific Ocean forced with climatological seasonally varying winds, equatorial upwelling and downwelling in adjacent latitudes play central roles in closing the oceanic circulation. The transport of the eastward North Equatorial Countercurrent decreases in a downstream direction because fluid is lost to downwelling into the thermocline where there is equatorward motion. Although this fluid converges onto the Equatorial Undercurrent, the latter's transport decreases because of equatorial upwelling. The upwelling, on the other hand, enhances the transport of the westward South Equatorial Current. Seasonally, the Countercurrent and South Equatorial Current are intense during the Northern Hemisphere summer and fall, at which time the thermocline has a pronounced trough near 3°N and a ridge near 10°N, and are weak in the spring when latitudinal thermal gradients are small and when the southeast trades are relatively weak. These variations are out of phase with those of the Equatorial Undercurrent, which is most intense in the spring.

The seasonal changes are associated with considerable variations in the meridional heat transport, especially across 9°N. The heat transport is always towards the winter hemisphere. During the northern winter, Ekman drift in the central Pacific affects the northward transport of warm surface waters. During the northern summer, when the ITCZ is near 9°N and the winds there are weak, the Ekman drift across 9°N is small. The relatively steady southward flow of warm surface waters across 9°N in the far western Pacific now contributes significantly to the southward heat transport. Seasonally there is both this meridional and a zonal redistribution of warm surface waters in the upper tropical Pacific Ocean. The zonal redistribution, from west to east, contributes to high sea surface temperatures in the east in April when the Equatorial Undercurrent surges eastward and attains its highest speed and transport during the period of weak southeast tradewinds. Increased heat flux across the ocean surface at this time also contributes to the warming of the upper equatorial ocean. Seasonal wind variations west of the dateline have little effect on the eastern tropical Pacific in the model.

1. Introduction

The salient features of the oceanic circulation in the tropics are the alternating bands of eastward and westward flowing currents: the westward North and South equatorial currents and the eastward North Equatorial Countercurrent and Equatorial Undercurrent (Fig. 1). The dynamics of each of these currents has been studied extensively but little attention has been paid to the relation between the currents, so that questions about the origin and fate of the waters in the various currents are unanswered. Data with which to address these questions are unavailable. The only manner in which to proceed is to use the limited available data together with a dynamical model. This is how Wyrtki (1981), Bryden and Brady (1985), and Enfield (1986) have attempted to estimate equatorial upwelling and to study the heat budget of the equatorial Pacific. They consider a volume of water that extends from 5°S to 5°N and from the dateline to the Galapagos Islands or 150° to 110°W in the case of Bryden and Brady (1985). The fluxes into and out of this volume are estimated by using wind stress data to calculate the meridional Ekman drift across 5°N and 5°S, and by using hydrographic data to infer geostrophic meridional and zonal currents. Inaccuracies arise because of the paucity of the data and because of the crudeness of the models. The hydrographic data do not resolve the very energetic 3-week instability waves which, in the eastern equatorial Pacific, affect the thermal field as much as the seasonal forcing does (Hayes et al., 1983). The assumption that the zonal flow near the equator is in geostrophic balance is sometimes valid but not where the winds have a cross-equatorial component that maintains a cross-equatorial pressure gradient in the thermocline. These studies probably yield reasonable estimates of gross quantities such as the volume of water transported upward across a horizontal surface at 100 m between 5°N and 5°S provided zonal variations are small, but for a detailed picture of the three-dimensional structure of the flow more sophisticated models than those used in these pioneering studies are required. The models should take into account the 3-week instability waves and the nonlinear dynamics near the equator, and should exploit more fully the information in the wind field, which does far more than drive Ekman drift. General Circulation Models meet these

* Present address: Climate Analysis Center, NMC/NWS/NOAA, Washington, DC 20233.

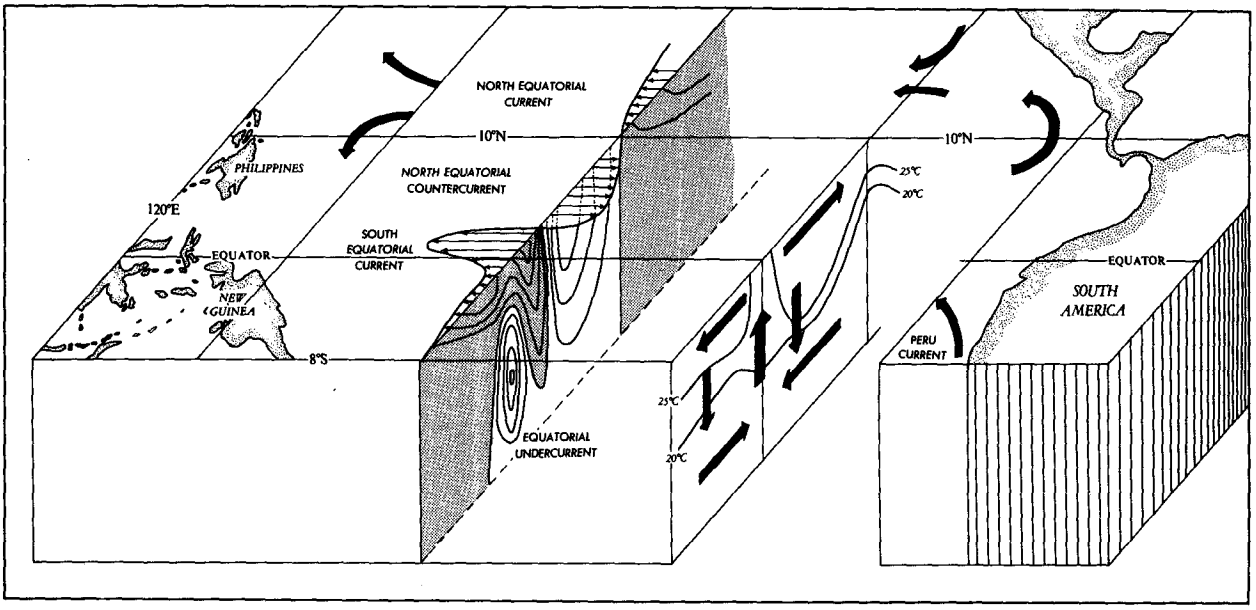

FIG. 1. A schematic diagram of the horizontal and vertical circulation in the tropical Pacific Ocean.

conditions and realistically reproduce conditions in the tropical oceans when forced with the observed winds (Philander and Seigel, 1985; Philander and Pacanowski, 1986; Richardson and Philander, 1987; Garzoli and Philander, 1985). This paper uses such a model (as described in section 2) to study the mass and heat budget of the tropical Pacific. The available data serve as initial conditions for the model. For the best possible dataset with which to study mass and heat budgets the oceanic measurement should be used not merely as initial conditions but should be assimilated into the model to mitigate its deficiencies, inaccurate forcing functions and inadequate parameterization of mixing processes. Models that run in this mode are not yet available.

2. The model

The Pacific Ocean model extends from 130°E to 70°W, and 28°S to 50°N. The coastlines and gridpoint distribution are shown in Fig. 2. The longitudinal resolution is a constant 100 km, but the latitudinal distance between gridpoints is 33 km between 10°S and 10°N and increases gradually poleward of this region.

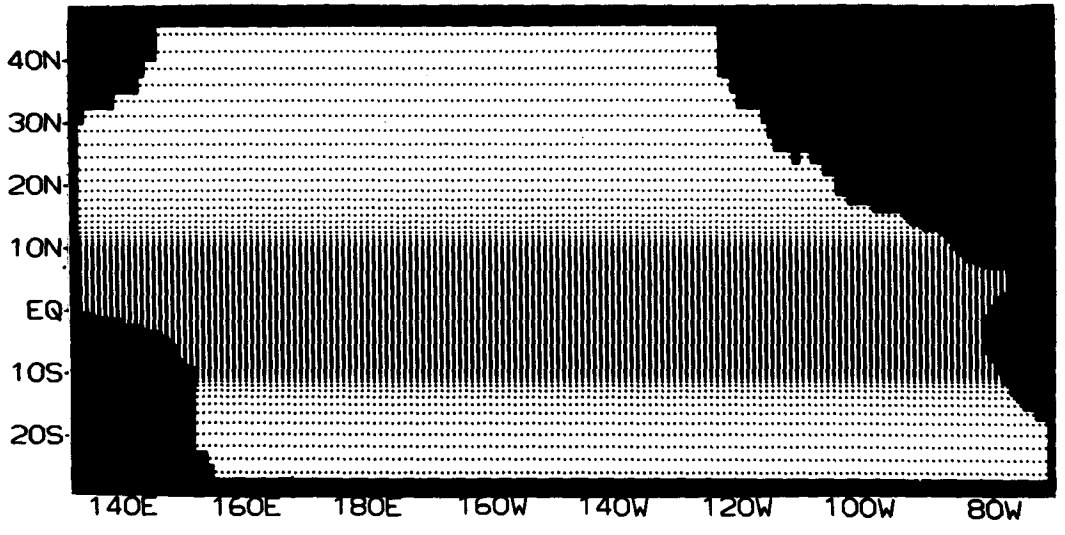

FIG. 2. The distribution of gridpoints and the idealized geometry of the model.

The spacing at 25°N is 200 km. The flat-bottom ocean is 4000 m deep. There are 27 levels in the vertical; the upper 100 m have a resolution of 10 m.

The primitive equations are solved numerically by means of finite-differencing methods discussed in Bryan (1969). The use of Richardson number dependent vertical mixing coefficients is explained in detail in Pacanowski and Philander (1981). In the upper 10 m of the model, the coefficient of vertical eddy viscosity has a minimum value of 10 $cm^2\ s^{-1}$ to compensate for mixing by the high-frequency wind fluctuations which are absent from the monthly mean winds. In the deep ocean where vertical mixing is negligible, vertical viscosity has the value of molecular viscosity. The coefficients of horizontal eddy viscosity and diffusivity are $1 \times 10^7\ cm^2\ s^{-1}$ equatorward of 10° latitude; poleward of this, they increase gradually to a value of $7 \times 10^7\ cm^2\ s^{-1}$ at 50°N. Unstable temperature gradients are eliminated instantaneously by mixing heat vertically to a depth that ensures a stable density gradient.

Poleward of 20°S and 30°N the equation for temperature T gains a term $\gamma(T - T^*)$ where T^* is the prescribed monthly mean climatological temperature for the region under consideration, and γ is a Newtonian cooling coefficient. Its value is $(2\ days)^{-1}$ near the zonal boundaries and decreases to a value of zero equatorward of 30°N and 20°S. This device mitigates the effect of the artificial zonal walls along the southern and northern boundaries of the ocean and forces the solution towards the climatology in these regions.

The heat flux across the ocean surface is

$$Q = \mathrm{SW} - \mathrm{LW} - \mathrm{QS} - \mathrm{QE}. \tag{1}$$

The solar shortwave heating SW is taken to be 500 ly day^{-1} equatorward of 20° latitude and decreases linearly to 300 ly day^{-1} between 20° and 45° latitude. The longwave back radiation LW has the constant value of 115 ly day^{-1}. The sensible heat flux is

$$\mathrm{QS} = \rho C_D C_p V(T_0 - T_A), \tag{2}$$

and the evaporation is

$$\mathrm{QE} = \rho C_D L V[e_s(T_0) - \Upsilon e_s(T_A)](0.622/p_A) \tag{3}$$

where the saturation vapor temperature is

$$e_s(T) = 10^{[9.4-(2353/T)]}. \tag{4}$$

Here $\rho = 1.2 \times 10^{-3}\ g\ cm^{-3}$; $L = 595\ cal\ g^{-1}$; $C_D = 1.4 \times 10^{-3}$; $p = 1013$ mb; $C_p = 0.24\ cal\ g^{-1}\ °C^{-1}$; T_0 is the sea surface temperature in degrees Kelvin; T_A is the atmospheric temperature at the surface; V is the surface wind speed; and the relative humidity Υ is assigned the constant value 0.8. No provision is made for clouds. The sensible heat flux is found to be of secondary importance so that variations in heat flux are primarily a consequence of change in the evaporation. Since evaporation depends on the wind speed, avoidance of excessively high temperatures in regions of weak winds required that the wind speed not be less than 4.8 $m\ s^{-1}$. This restriction applies only to the evaporative term where evaporation caused by high-frequency wind fluctuations is otherwise lost by the use of mean monthly winds.

The initial conditions for the model are zero currents and the climatological temperature and salinity fields of January (Levitus, 1982). Monthly averaged climatological winds (Hellerman and Rosenstein, 1983) then force the model for two years by which time the model has an equilibrium seasonal cycle. The results to be shown here are from the third year of the simulation. Experiments to determine how different initial conditions affect simulations indicate that the upper tropical Pacific takes on the order of a year to "forget" initial conditions (Philander and Hurlin, 1987). The adjustment time for the region below the thermocline is longer.

3. The mean circulation and its seasonal variation

The mean circulation is characterized by the currents depicted schematically in Fig. 1. To determine how this circulation is closed, the model ocean was divided into the boxes shown in Fig. 3. A triad of numbers in this figure denotes the annual mean horizontal mass fluxes (in Sverdrups) across a vertical surface in the upper 50 m, between 50 and 317 m, and below 317 m, respectively. A minus sign means that the flux is opposite to the direction of the arrow. (The chosen circles of latitude in Fig. 3 do not exactly coincide with the boundaries between the various currents, but the currents will nonetheless be referred to by their usual names.) The numbers in the circles in Fig. 3 give the vertical transports, also in sverdrups ($Sv \equiv 10^6\ m^3\ s^{-1}$), across 50 and 317 m, respectively. A plus sign indicates upwelling. The eastward Countercurrent is seen to be convergent and is associated with a downwelling of surface water. As it flows eastward, this current loses mass because of northward Ekman drift across 10°N and equatorward flow at the depth of the thermocline across 2.5°N. This equatorward flow into the Equatorial Undercurrent is supplemented by a similar flux across 2.5°S, but the transport of the Undercurrent nonetheless decreases in a downstream direction because of intense equatorial upwelling. Poleward Ekman drift carries this upwelled water to the South Equatorial Current which advects it westward. In the far western Pacific, west of 150°E, some of the westward flow north of 10°N, and some of that in the South Equatorial Current, converge in order to maintain the two eastward currents (Hasunuma and Yoshida, 1978).

Upwelling at the equator and downwelling in the neighboring latitudes play important roles in closing the oceanic circulation. The vertical structure of the mean vertical velocity component (Fig. 4) indicates equatorial upwelling at all meridians, even in the west where the thermocline is deepest. The upwelling is

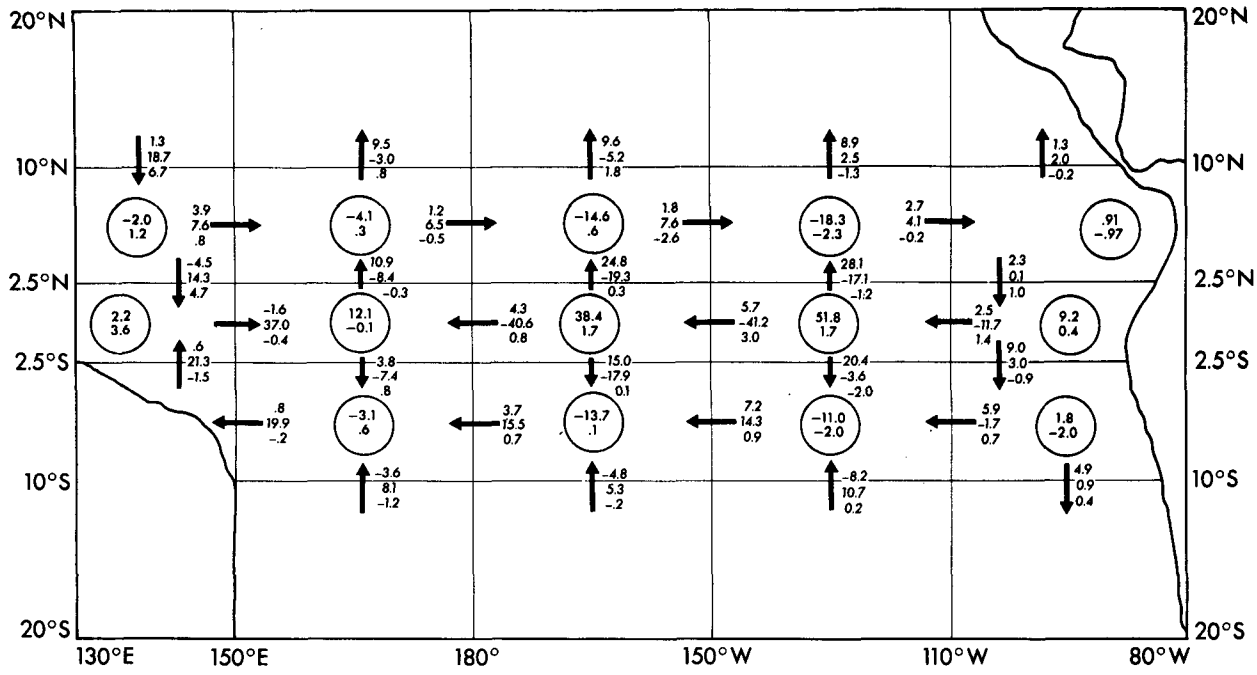

FIG. 3. The mass budget. A triad of numbers indicates the horizontal mass transport (Sv) across the upper 50 m, between 50 and 317 m, and below 317 m respectively, of the indicated vertical plane. A negative sign means that the transport is opposite to the direction of the arrow. Numbers in the circles indicate the upward mass flux (if positive) across the 50 m and 317 m surface, in 10^3 m^3 s^{-1}.

confined to the upper ocean and does not penetrate to depths greater than approximately 150 m. The adjacent downwelling (Fig. 4, right-hand panel) is more intense to the north of the equator than to the south, especially in the central Pacific.

Seasonal variations of the surface winds over the tropical Pacific Ocean are associated with the seasonal migrations of the Intertropical Convergence Zone (ITCZ) onto which the northeast and southeast trades converge. During the Northern Hemisphere spring, the

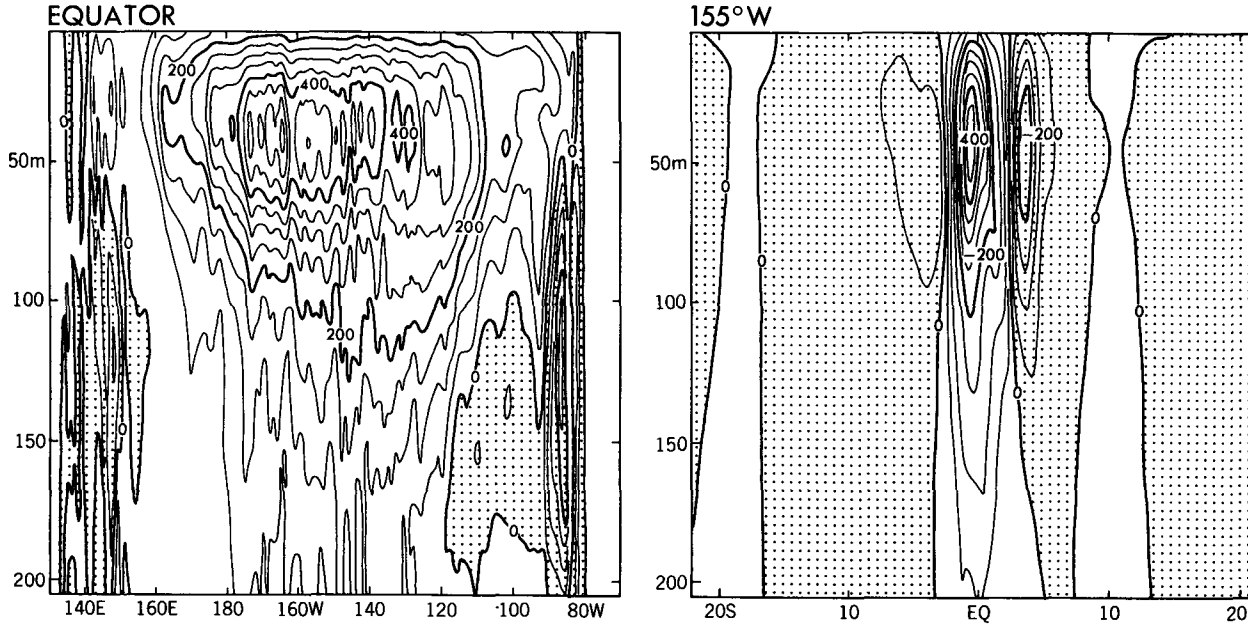

FIG. 4. The annual mean vertical velocity component along the equator and along 155°W in units of cm day^{-1}. Shaded areas indicate downwelling.

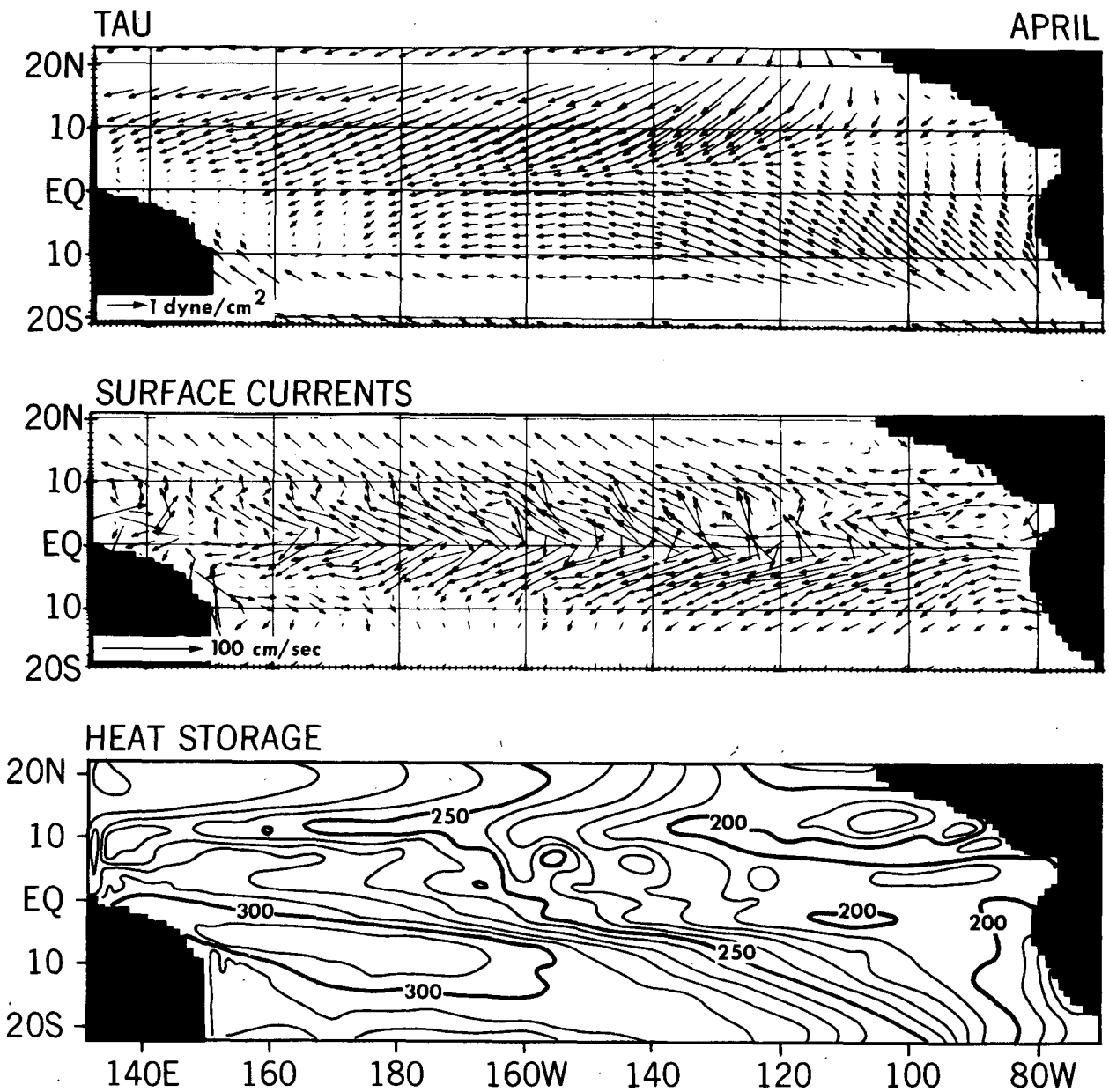

FIG. 5. The surface winds and currents, and the vertically integrated temperature (over the upper 317 m of the model) in units of 10^3 cal cm^{-2} in April and October.

ITCZ is near the equator and the southeast trades are weak. During the Northern Hemisphere autumn, the ITCZ is farthest north and the southeast tradewinds are most intense. These changes in the windstress pattern and the associated changes in the thermal structure of the ocean and in the surface currents are shown in Fig. 5. During the period of relaxed equatorial winds (March–May), the surface currents are weak and generally westward while horizontal thermal gradients are at a minimum. Intensification of the southeast trades strengthens the westward surface flow near the equator and also brings to the surface the eastward Countercurrent, between approximately 3°N and 10°N. The Countercurrent is associated with a pronounced ridge of the thermocline near 10°N and a trough near 3°N, as can be seen in Figs. 5 and 6. It follows that changes in the elevation of the thermocline at these two latitudes are out of phase, as is evident in Fig. 7. A preliminary analysis of the results indicate that thermal variations, at and north of 10°N, are in response to changes in the local wind-induced Ekman pumping, in agreement with Meyers' (1979) data analysis. South of 9°N, matters are more complex. Both the wind stress curl and the cross-equatorial component of the wind contribute

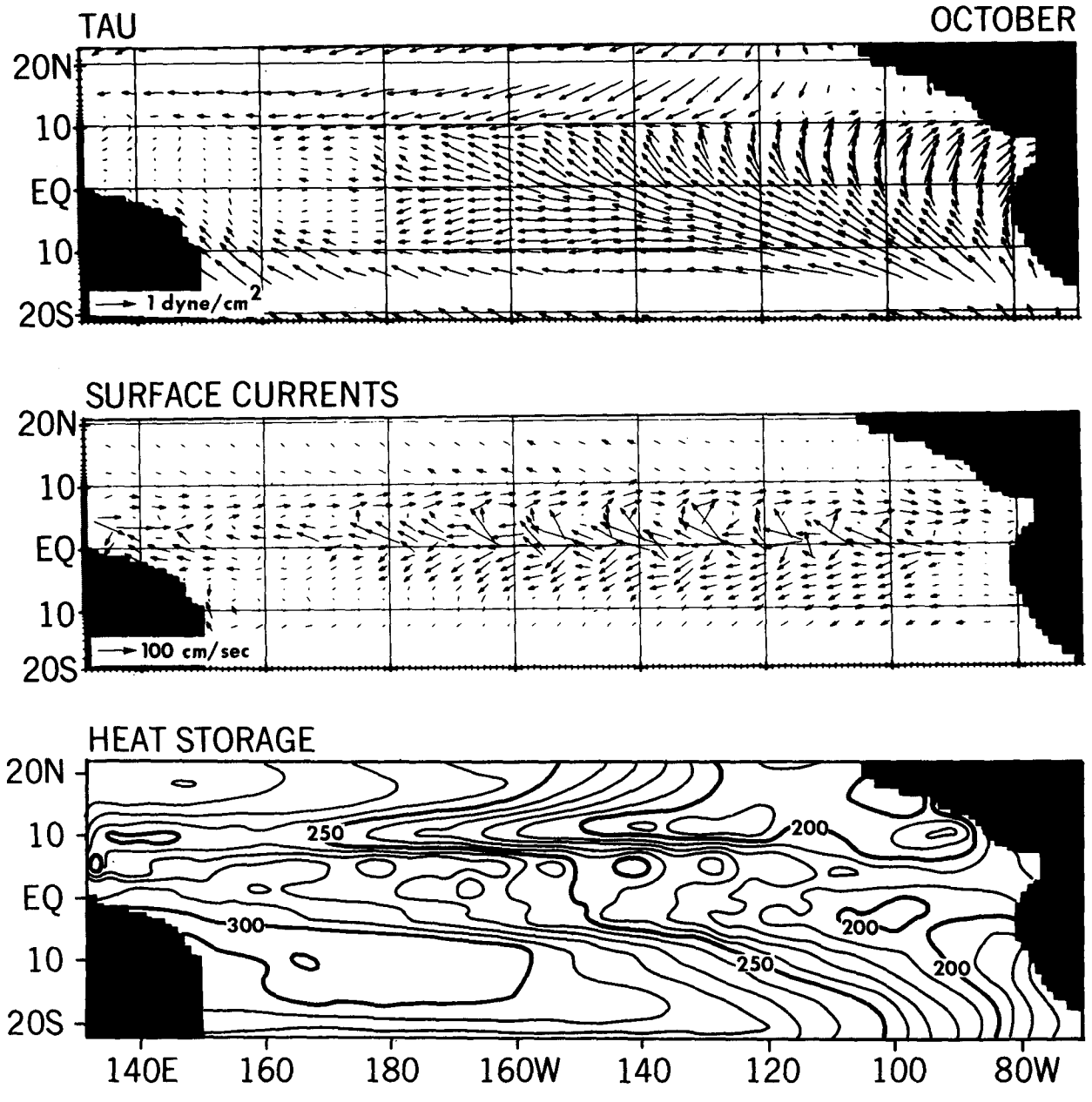

FIG. 5. (*Continued*)

to the downwelling which is most intense in the trough of the thermocline near 3°N. The westward Ekman drift, driven by the northward winds south of the equator, is advected across the equator (Cane, 1979) to the region of downwelling so that the westward current penetrates to considerable depths north of the equator (Fig. 6). Thus, the northward component of the wind contributes significantly to the asymmetries about the equator in Fig. 6.

A more detailed study of the dynamics of the North Equatorial Countercurrent, and the role that waves play in its adjustment to seasonal changes in the winds, will be presented on another occasion. It is of considerable interest that a linear shallow water model simulates the seasonal variations of the Countercurrent fairly well (Busalacchi and O'Brien, 1980). A comparison of those results with results from the general circulation model will shed light on the effect mean currents have on oceanic adjustment.

The time series of the surface currents in the central Pacific (Fig. 7) show that the seasonal changes are non-sinusoidal, that they have their largest amplitude between the equator and 10°N, and that there are energetic fluctuations with a period of approximately one

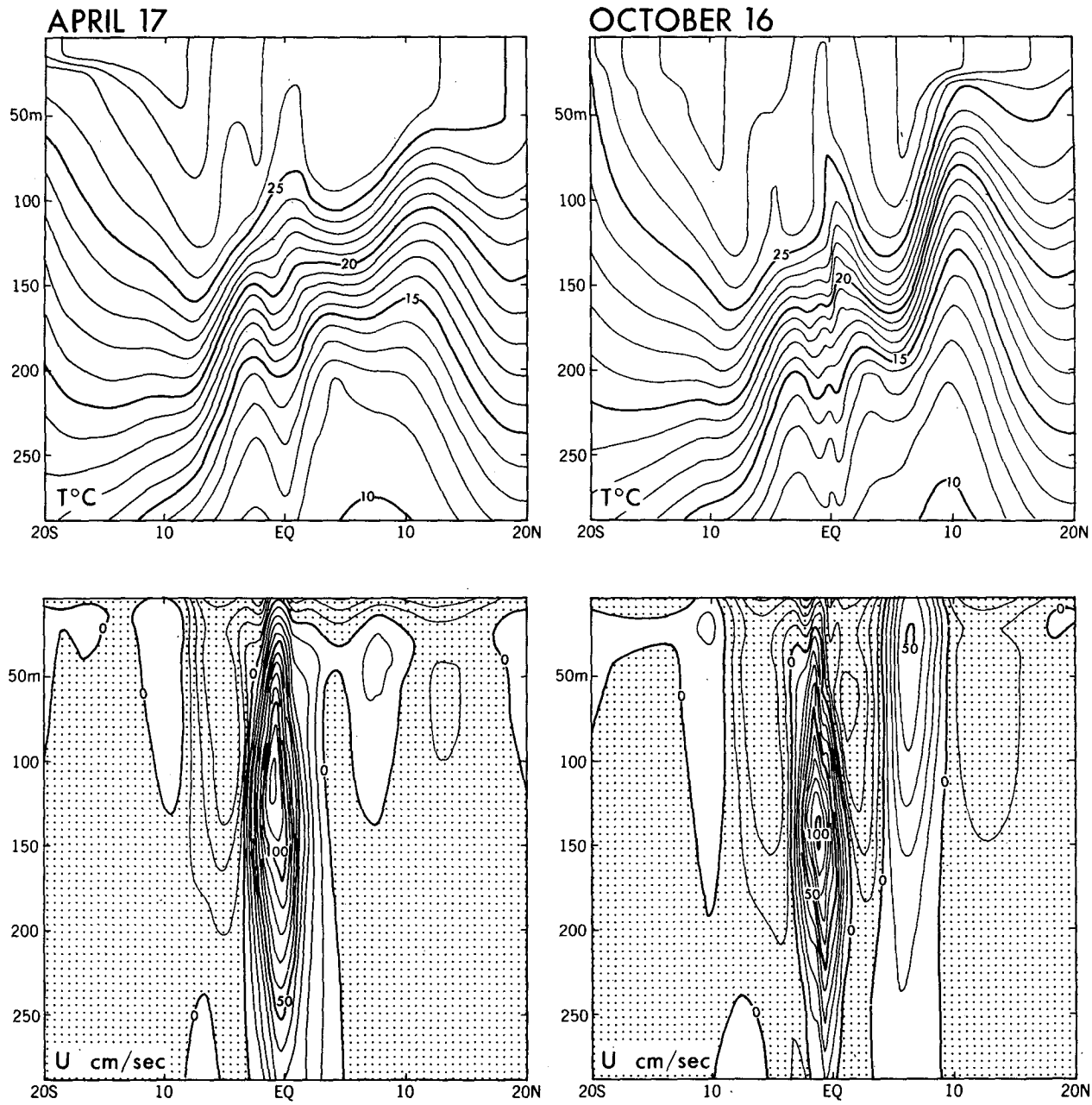

FIG. 6. The zonal currents across 160°W and the temperature (°C) along that meridian. Flow is westward in shaded areas; the contour interval is 10 cm s^{-1}.

month. The properties of these high-frequency fluctuations, which are caused by instabilities of the mean currents, especially the westward jet to the north of the equator, are discussed elsewhere (Philander et al., 1986). These waves affect the transports of the various currents (Fig. 8). (In this figure the domains of the currents are taken to be the following: the region of westward flow between 6°N and 10°S, and between the surface and 317 m for the South Equatorial Current; the region of eastward flow above 317 m and between 3°N and 10°N for the North Equatorial Countercurrent; and the region of eastward flow above 317 m and between 3°N and 3°S for the Equatorial Undercurrent.) The surface currents are found to be most intense when the transport of the Equatorial Undercurrent is at a minimum, during the Northern Hemisphere autumn. The situation is reversed in the spring when the Undercurrent transport is large and that of the surface currents is small. The mass budget changes in an interesting way between autumn and spring, especially

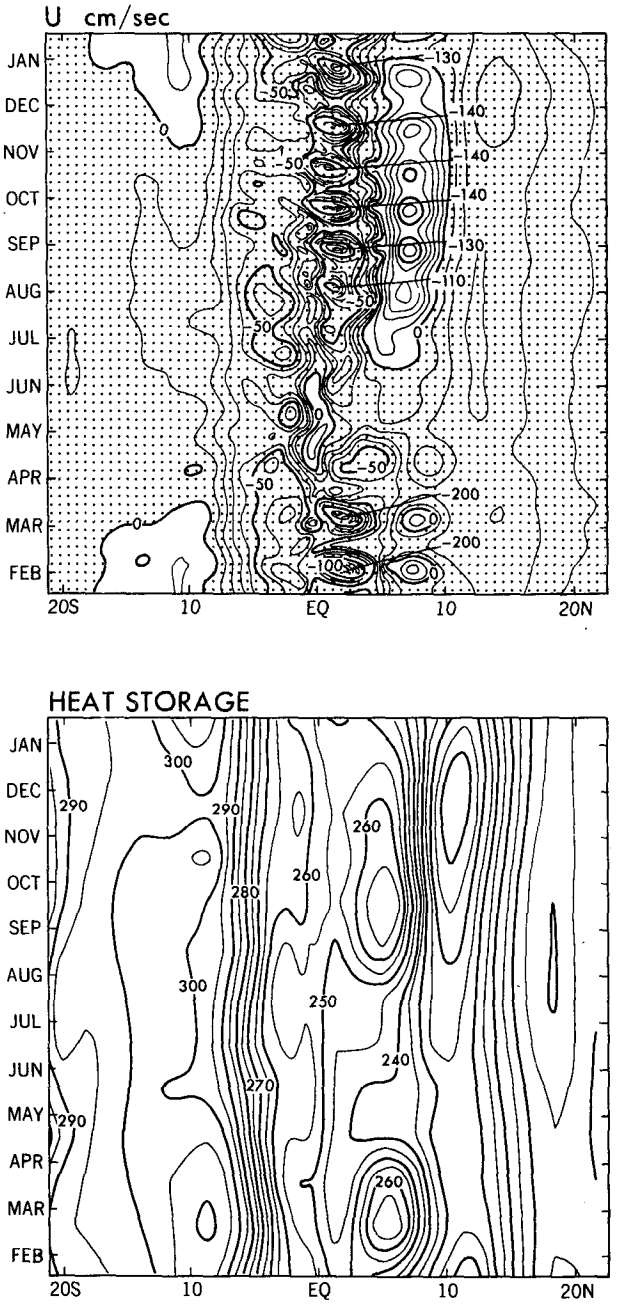

FIG. 7. Seasonal variations of the zonal surface current across 155°W and the vertical integral of the temperature along 155°W. Motion is westward in shaded areas. The contour interval is 10 cm sec^{-1} for the current, 10^3 cal cm^{-2} for the heat storage.

in the eastern half of the basin where zonal gradients are large. The ITCZ is furthest north in late summer and fall so that the southeast trades near the equator are intense but the winds near 10°N, near the ITCZ, are weak. Poleward Ekman drift is therefore large across 2.5°N but is small across 10°N (Fig. 9a). This convergent meridional flow in the surface layers is associated with intense downwelling in the region of the Countercurrent. Much of this water flows equatorward, into the Equatorial Undercurrent, at the depth of the thermocline as shown in Fig. 9b. The fluid that converges on the equator at depth, and to a lesser extent the downstream decrease in the transport of the Equatorial Undercurrent, sustains the intense equatorial upwelling. In the surface layers of the equatorial zone, between 2.5°N and S above 50 m, the mass balance is two-dimensional with upwelling balancing poleward drift.

When the southeast trades are relaxed, in the Northern Hemisphere spring, the mass balance in the surface layers of the equatorial zone remains two-dimensional but matters are very different in the Countercurrent and Undercurrent. The poleward Ekman drift now barely changes between 2.5° and 10°N so that downwelling in the Countercurrent—this current practically disappears at this time—is at a minimum. The deep equatorward flow towards the Equatorial Undercurrent is also minimal (Fig. 9b). The weakened equatorial upwelling is now maintained principally by the downstream decrease in the transport of the Equatorial Undercurrent. This happens because the seasonal eastward surge of the Equatorial Undercurrent is far larger in the central Pacific, across 154°W, than in the east, across 110°W (Fig. 8).

The seasonal change in the meridional circulation is most clearly seen by introducing a streamfunction after integrating the continuity equation across the width of the basin (Fig. 10) depicts this streamfunction

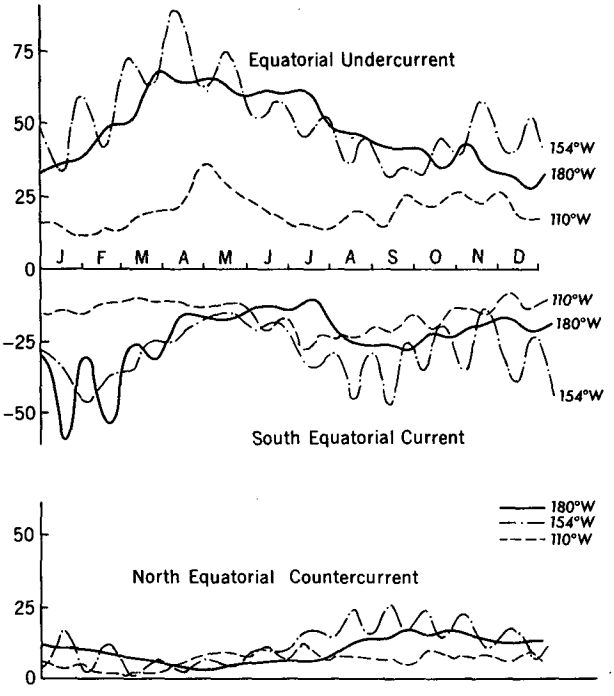

FIG. 8. Transports (in 10^6 m^3 s^{-1}) of the zonal currents across 180°, 155° and 110°W as a function of time. The domains of the currents are defined in the text.

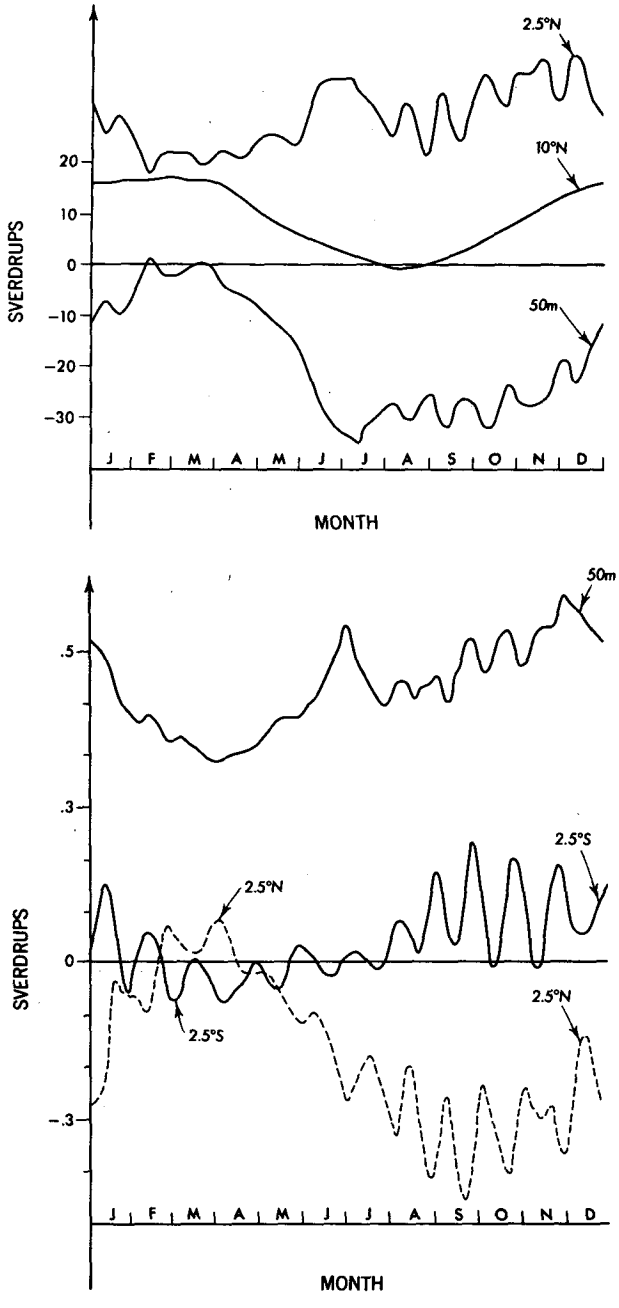

FIG. 9. (a) The northward mass flux (in 10^6 m^3 s^{-1}) across 2.5° and 10°N between 150° and 110°W in the upper 50 m of the model, and the upward mass flux across 50 m between the latitudes and longitudes just mentioned. (b) The northward mass flux (in 10^6 m^3 s^{-1}) across 2.5°S and 2.5°N between 150° and 110°W at depths below 50 and 317 m, and the upward mass flux across 50 m from this volume.

in April and September. Seasonal changes are modest to the south of the equator. North of the equator the poleward Ekman drift, which is fed by equatorial upwelling, is almost nondivergent in April but is strongly convergent in October when downwelling in the region of the Countercurrent is intense.

4. The equatorial zone

The equatorial zone, within a few hundred kilometers of the equator, is strongly influenced by the zonal component of the wind which, in the Pacific, is westward except near the eastern and western boundaries of the basin (Fig. 11). Away from the coasts, the westward wind has a very large annual mean value and relatively little variability about the mean. The thermal structure along the equator is similarly dominated by a large mean zonal gradient and relatively little temporal variability. Figure 11 shows a warming of the upper ocean in the eastern side of the basin in May and June, and a much weaker warming again in November. A semiannual signal is evident in the zonal winds, too, as has been noted before by Busalacchi and O'Brien (1980). Although the variability of the winds and thermal field along the equator is modest, the intensity of the surface currents fluctuates enormously (Fig. 11). There are a few months of weak eastward surface flow starting in April but by September, the westward current attains speeds in excess of 1 m s^{-1}. The vertical structure of these changes (Fig. 12) indicates that the eastward surface flow during the Northern Hemisphere spring is a surfacing of the Equatorial Undercurrent, which attains speeds of 150 cm s^{-1} and which penetrates right to the South American coast at this time. The maximum speed of the Undercurrent is far less in the autumn when it barely penetrates beyond 100°W. The surge of eastward flow along the equator in the spring is simultaneous with the warming of the upper layer of the eastern equatorial Pacific mentioned earlier. It also coincides with a period of relaxed westward winds in the neighborhood of 130°W (Fig. 11). These winds were maintaining an eastward pressure force. When the winds relax, the pressure force causes eastward acceleration. Kelvin waves are involved in this oceanic adjustment but are difficult to discern because of the complex temporal and spatial structure of the changes in the winds. In an experiment in which the winds are kept steady from 15 February onward, the eastward surge of warm water is absent so that the relaxation of the winds in March and April must be the cause of the surge (Fig. 13). The subsequent deceleration (or westward acceleration) is attributable to the intensification of the winds in June and not to reflected Rossby waves, because there is very little deceleration when the winds remain steady after 15 May (Fig. 13). It is possible for the westerly winds west of the dateline from November onward (Fig. 11) to contribute to the eastward surge of warm water in the east in April and May. To explore this possibility, we made a calculation in which the zonal winds west of the dateline were set equal to −0.2 dyn cm^{-2} whenever they exceeded that value. This meant that the eastward winds in the west were replaced by steady westward winds. The time and depth dependence of the motion in the eastern equatorial Pacific were practically unaf-

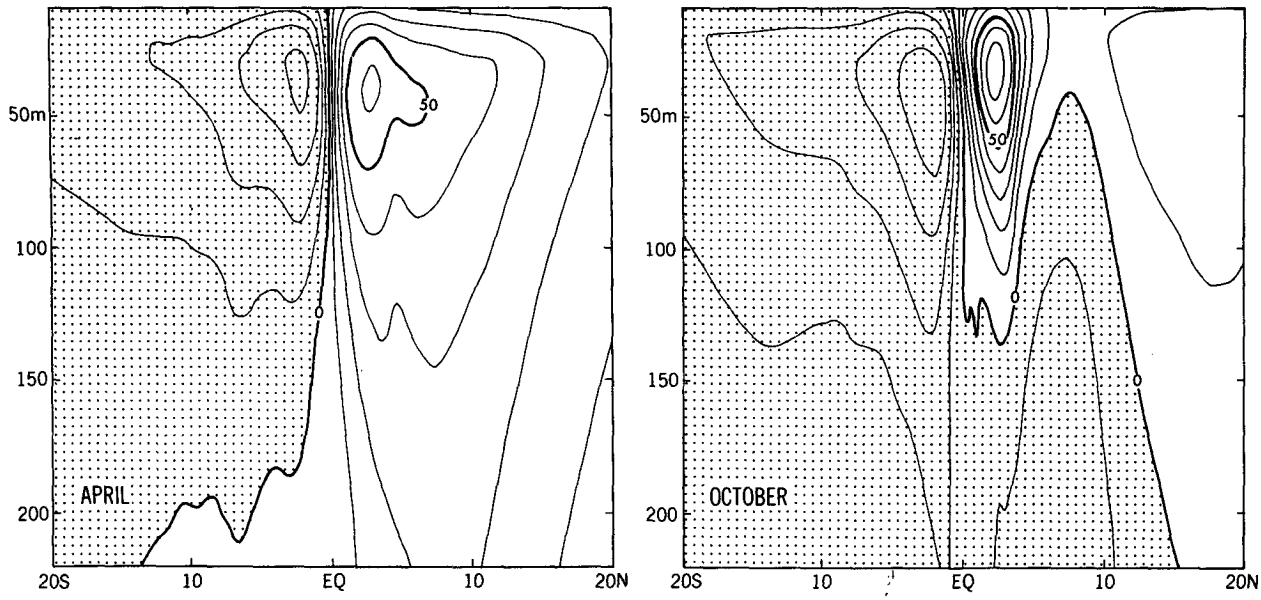

FIG. 10. The streamfunction, for the zonally integrated meridional circulation, on 17 April and 16 October. The contour interval is Sv $\equiv 10^6$ m^3 s^{-1}.

fected by the change in the winds. Cane and Moore (1981) have argued that gradually varying winds in the western side of a basin will merely affect the height of the thermocline in the east. Short bursts of winds that last a week or two west of the dateline will have a more noticeable effect on the currents in the east. The model, however, is forced with monthly mean winds so that such bursts are absent. Under such conditions, the eastward surge of warm water in the eastern Pacific in April and May is caused by the relaxation of the tradewinds over the central equatorial Pacific during the Northern Hemisphere spring.

5. The western equatorial Pacific

The vicinity of the equator is very sensitive to variations in the zonal component of the wind. On the time scale of a week, winds parallel to the equator can generate an intense equatorial jet in the direction of the wind. On a time scale of a month, the winds will maintain a zonal pressure gradient which can drive an equatorial undercurrent in a direction opposite to that of the wind. This means that fluctuations and reversals of the zonal component of the wind along the equator can result in currents with a complex vertical and temporal structure. Nonlinearities influence this structure because they intensify the eastward currents, and weaken westward currents (Philander and Pacanowski, 1980). The western equatorial Pacific is a region where the zonal component of the winds reverses direction seasonally, and where the currents have a complex structure. Hisard et al. (1970) report observations of westward surface flow and eastward subsurface currents with two distinct maxima on the equator near 160°E in March 1967, when the winds were westward. A month later, when the winds were eastward, they observed an eastward surface current separated from a deep eastward Equatorial Undercurrent by a westward current. Figure 14 shows examples of currents with such structures in the model. The currents in the upper 100 m are in response to the local winds. The eastward equatorial surface jet in December is driven by the local eastward winds at that time. There are remnants of this jet near 50 m in January when the local winds are westward. These currents across 160°E are near the boundary that separates regions of easterly and westerly winds along the equator (Fig. 11). It is for this reason that the variability of currents across 160°E is particularly complicated. There is currently a field program in the western equatorial Pacific that will provide measurements of the currents in that region over an extended period. The model will have to be improved—a more realistic geometry for the western Pacific, and forcing with the winds observed during the period of the measurements are essential—before a comparison between the measurements and the model results is attempted. A comparative study of equatorial currents in the western equatorial Pacific and eastern equatorial Indian Ocean when the winds and currents also have considerable variability (Taft, 1967) would be valuable.

6. The heat budget

Near the equator the ocean gains heat across its surface throughout the year, but in higher latitudes it loses more heat during summer than it gains during winter. To achieve a balance, the oceanic currents in the Pacific transport heat poleward from the equator. In the model

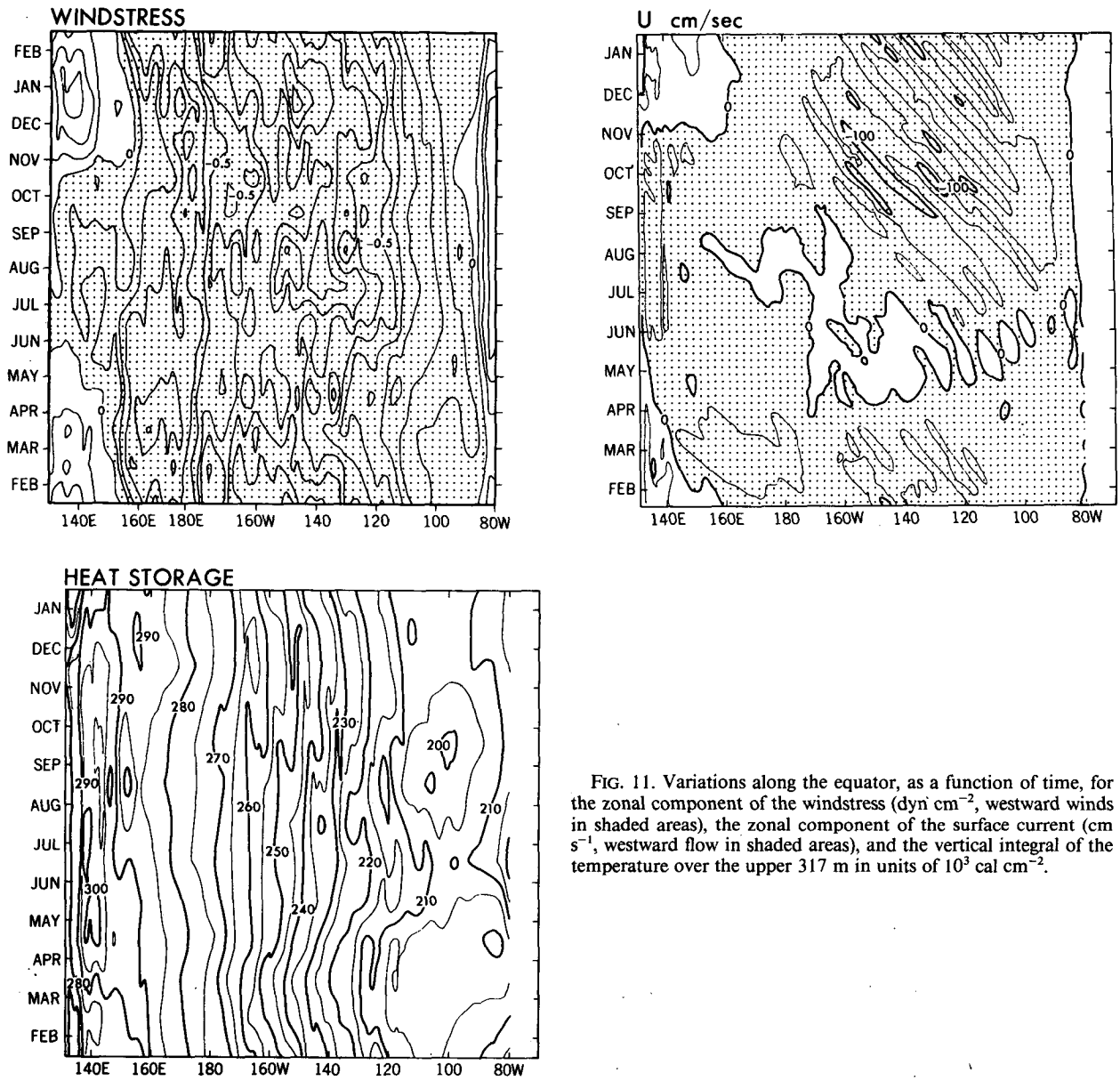

FIG. 11. Variations along the equator, as a function of time, for the zonal component of the windstress (dyn cm^{-2}, westward winds in shaded areas), the zonal component of the surface current (cm s^{-1}, westward flow in shaded areas), and the vertical integral of the temperature over the upper 317 m in units of 10^3 cal cm^{-2}.

the heat flux across the ocean surface is determined by the simulated sea surface temperatures and the specified air temperature and windspeed, as explained in section 2. This heat flux (Fig. 15) is in reasonable agreement with estimates based on oceanic and atmospheric data, especially if it is kept in mind that the data may be subject to considerable errors (Enfield, 1986). Figure 16 shows that the heat gained near the equator is transported predominantly northward. The shape of this curve depends entirely on the heat flux across the ocean surface when horizontal diffusive processes are neglected. This follows from the equation for the conservation of heat which, after vertical integration through the water column and zonal integration across the width of the basin, can be written

$$Q_t + (\mathrm{HT})_y = \text{Flux across the surface} + \text{diffusion}. \quad (5)$$

Here Q_t is the rate of change of heat storage and $(\mathrm{HT})_y$ is the divergence of the meridional heat transport. In a steady state the heat transport is known once it is specified at one latitude. In the model the boundary conditions at the artificial walls along 30°S and 50°N (there the imposed conditions correspond to the historical hydrographic data) in effect determine the results shown in Fig. 16. In a similar exercise for the Atlantic Ocean, the results are quite different because the heat transport is found to be northward in both hemispheres (Philander and Pacanowski, 1986). The flux across the surface in the equatorial Atlantic augments the northward heat transport. This difference between the mod-

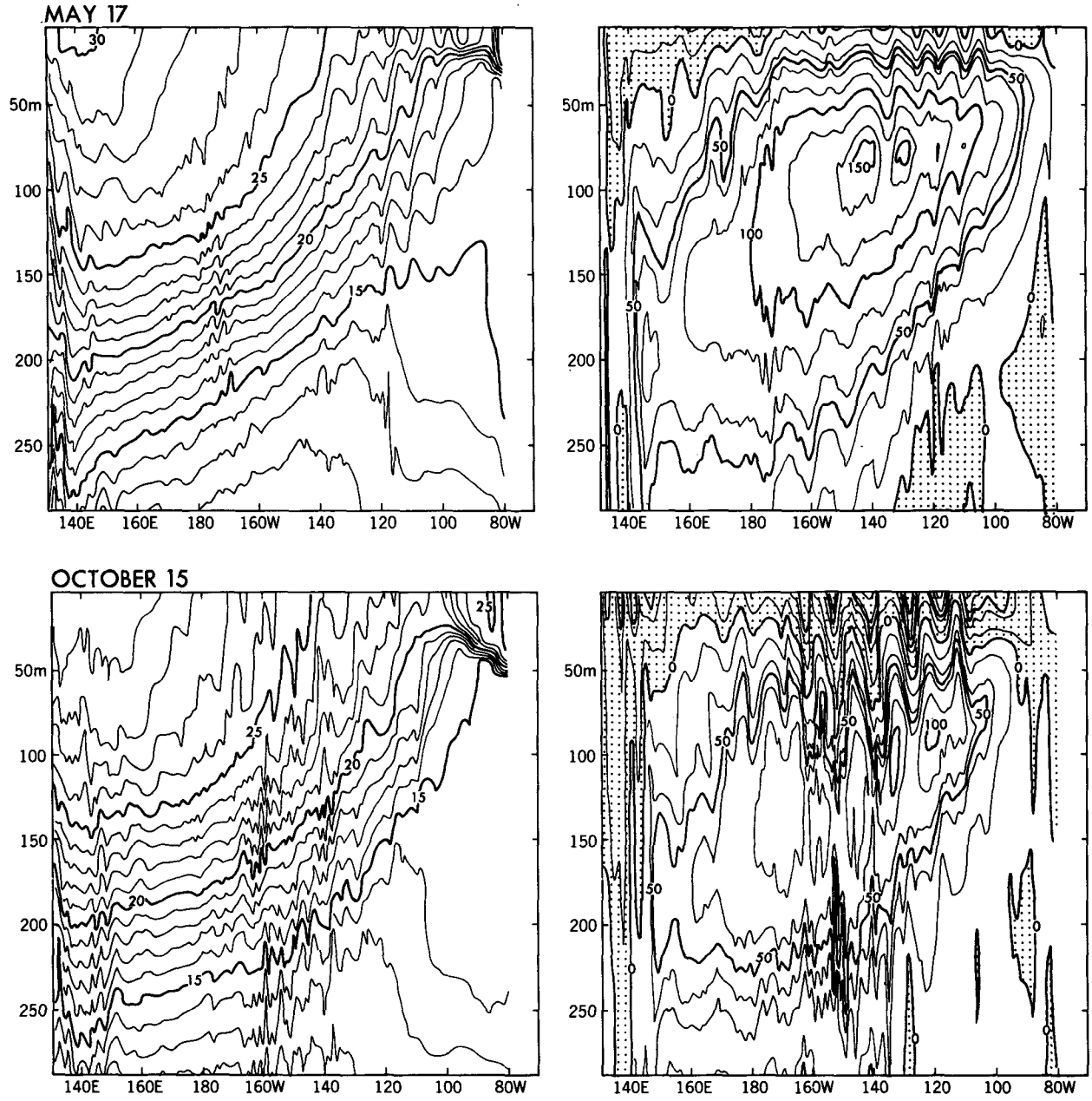

FIG. 12. Sections along the equator on 17 May and 15 October of the zonal current (cm s^{-1}, westward flow in shaded areas) and of the temperature (°C).

els for the Atlantic and Pacific is in agreement with inferences drawn from measurements (Bryan, 1982).

To study the annual mean heat budget in more detail we calculated the advection of heat across the different surfaces shown in Fig. 17. A triad of numbers indicates the horizontal advection of heat, in petawatts, across the upper 50 m, between 50 and 317 m, and below 317 m. A minus sign means that advection is opposite to the direction of the arrow. In the circles, the upper number indicates the heat flux across the ocean surface into the ocean if positive; the two lower numbers indicate the vertical advection across 50 and 317 m, respectively, and is positive if upward. The heat budget of the equatorial zone, characterized by a tongue of cold surface waters, is of special interest. Figure 17 indicates that the dominant terms in the equation for the conservation of heat in the upper 50 m of the equatorial zone are those associated with the meridional circulation. The terms $(vT)_y$ and $(wT)_z$ far exceed the term $(uT)_x$ and the flux across the surface in the upper equatorial zone. [Here (u, v, w) are the velocity components in the zonal x, meridional y and vertical z

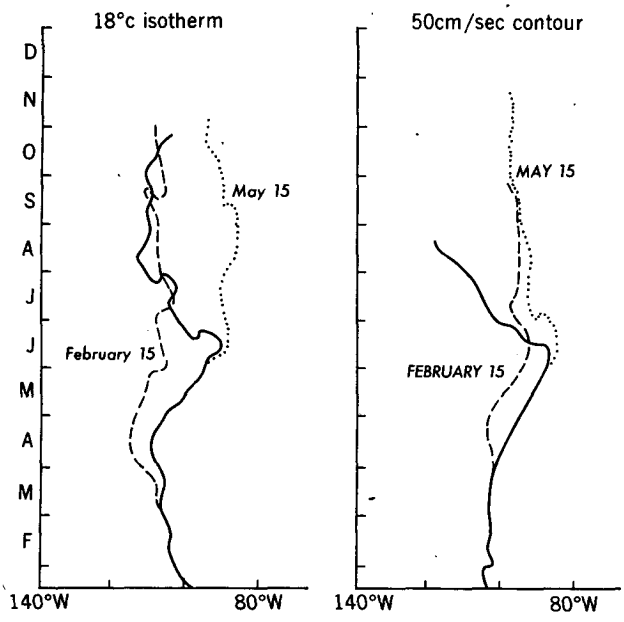

FIG. 13. The 18°C isotherm and 50 cm s^{-1} contour of the zonal current, at a depth of 55 m on the equator for the standard seasonal simulation and for two additional cases. In one case, the winds were held constant from 15 February onwards, in the other, from 15 May onwards.

directions, and T denotes temperature.] In other words, the low sea surface temperatures at the equator are caused by local upwelling, not by westward advection of cold surface waters. Note that the sum, $(vT)_y + (wT)_z$, is actually smaller than the terms $(uT)_x$ and the flux through the surface. This means that the three-dimensional divergence of the heat flux approximately balances the flux through the surface. In practice, this divergence is extremely difficult to calculate because it involves the small difference between two large terms associated with upwelling and poleward Ekman flow. Equatorward flow between 50 and 317 m compensates for the poleward surface flow. Between the dateline and 150°W, the deep equatorward advection maintains the equatorial upwelling. Farther east, the deceleration of the Equatorial Undercurrent makes the term $(uT)_x$ important in the equation for the conservation of heat. The balance for each box in Fig. 17 is not exact because diffusion has not been taken into account. Its contribution is much smaller than that of the terms that are shown. Effective meridional diffusion associated with the waves caused by instabilities of the mean currents is taken into account in Fig. 17 because the waves are resolved by the time-series data that are used to calculate the annual mean values. These waves are important primarily between the equator and 3°N in the upper 50 m of the central and eastern Pacific where their equatorward heat flux is comparable in magnitude to the flux across the ocean surface (Philander et al., 1986).

The meridional heat transport (HT) was huge seasonal variations and is always towards the winter hemisphere (as shown in Fig. 18). The divergence of this transport $(HT)_y$ is almost unrelated to the heat flux across the ocean surface in Fig. 19, but it is highly correlated with the rate of change of heat storage. In other words, the two terms on the left-hand side of Eq. (5) are essentially in balance on a seasonal timescale.

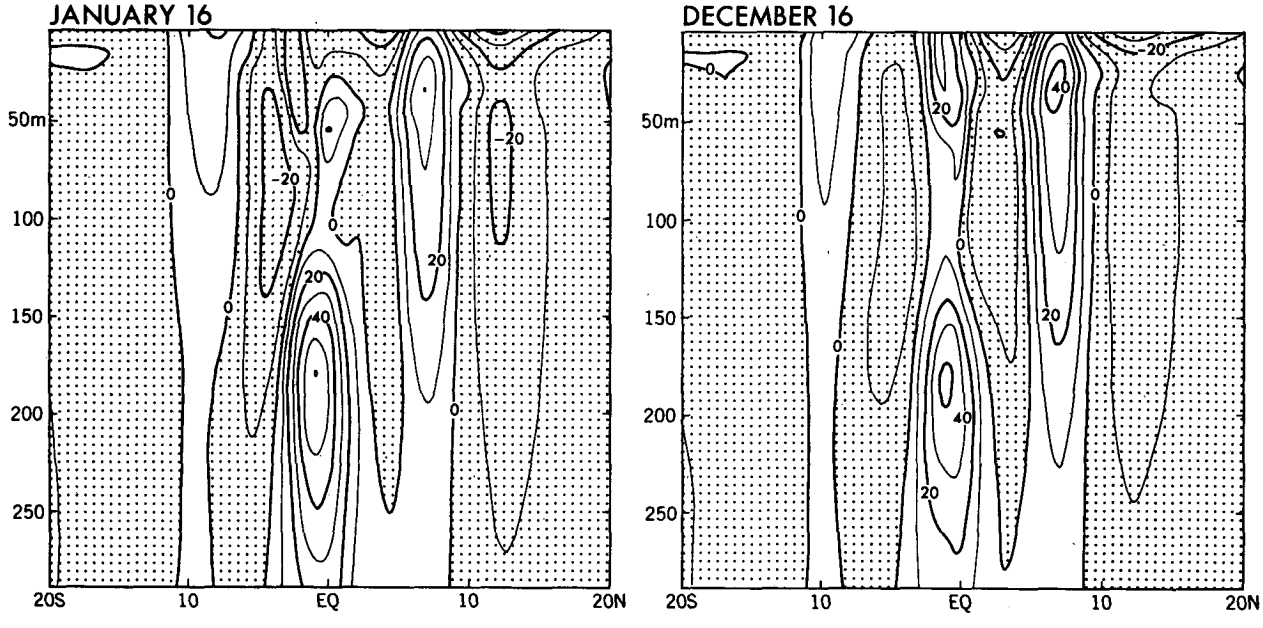

FIG. 14. Sections along 161°E of the zonal current (cm s^{-1}, westward flow in shaded areas) on 15 December and 15 January.

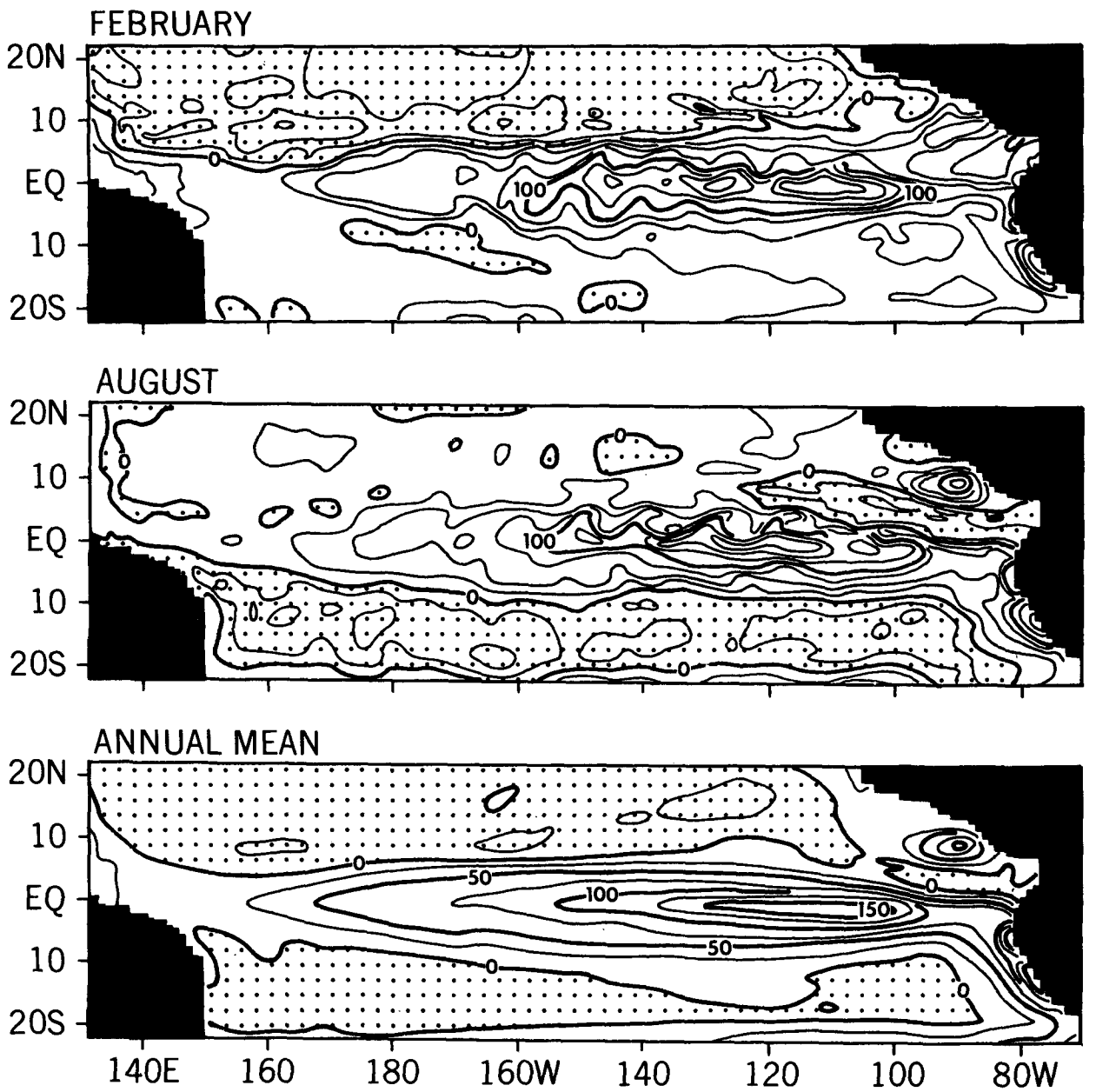

FIG. 15. The heat flux across the ocean surface (W m^2, upward out of the ocean in shaded areas) during February, August, and averaged over a year.

(For the annual mean, the first term is zero and the divergence of the heat transport is equal to the flux across the surface.) The structure of the rate of change of heat storage Q_t (Fig. 20) is almost identical to that of $(HT)_y$ except for having a different magnitude. The difference, which is essentially the heat flux shown in Fig. 19, has relatively little time dependence near the equator. This explains why in adiabatic models (Pares-Sierra et al., 1985), the rate of change of heat storage has a structure very similar to that in Fig. 20. The adiabatic models provide a picture of seasonal changes in $(HT)_y$ that is qualitatively, but not quantitatively, correct. For example, the large increase in the heat storage of the equatorial zone in April in Fig. 20 is attributable primarily to the flux across the ocean surface at that time (Fig. 19). The diabatic terms on the right-hand side of Eq. (5) clearly are not negligible.

Variations in the meridional heat transport have their largest amplitude near 9°N where the heat transport is 4×10^{15} W in February, -2×10^{15} W in September. In Fig. 20, 9°N is essentially a nodal line for heat storage variations which are of the opposite sign

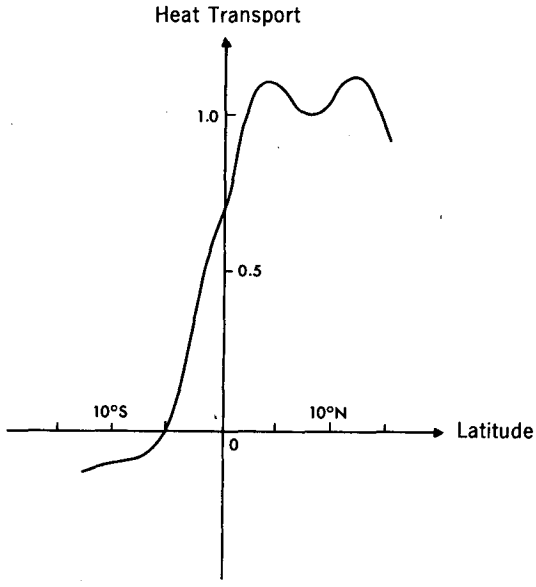

FIG. 16. The annual mean northward heat transport (in units of 10^{15} W) in the model.

on the two sides of this latitude. Between December and May the northward heat transport across 9°N increases the heat stored north of this latitude at the expense of the region to the south. Latitudinal thermal gradients are weak at this time, so that the countercurrent is relaxed, and the northward Ekman drift across 10°N in Fig. 9a is at a maximum. From July through October the trough of the thermocline near 3°N deepens considerably and the countercurrent intensifies. The heat storage south of 9°N now increases, while that of the region further north decreases. Exactly where does this warm water flow southward? It is not in the central Pacific because the Ekman drift across 10°N in Fig. 9a is small, nonnegative and southward. Figure 17 shows that the far western Pacific, where the thermocline is deep, has a southward transport of warm water across 10°N. Much of this southward flow is in a current along the western boundary. Seasonal changes in the transport of this current, the model's version of the observed Mindanao Current, are small. When the northward Ekman flux across 10°N in the central Pacific is large, the associated heat transport exceeds the southward transport in the far west, but when it is small or zero the net transport across 10°N is determined by what happens in the west. It follows that from June to October, the deepening of the thermocline south of 9°N and its shoaling further north involve both a zonal and a meridional redistribution of heat and in addition, involve diabatic processes. The meridional redistribution across 9°N is primarily in the western Pacific; the zonal (eastward) redistribution is by means of the North Equatorial Countercurrent, which intensifies during these months, and the Equatorial Undercurrent.

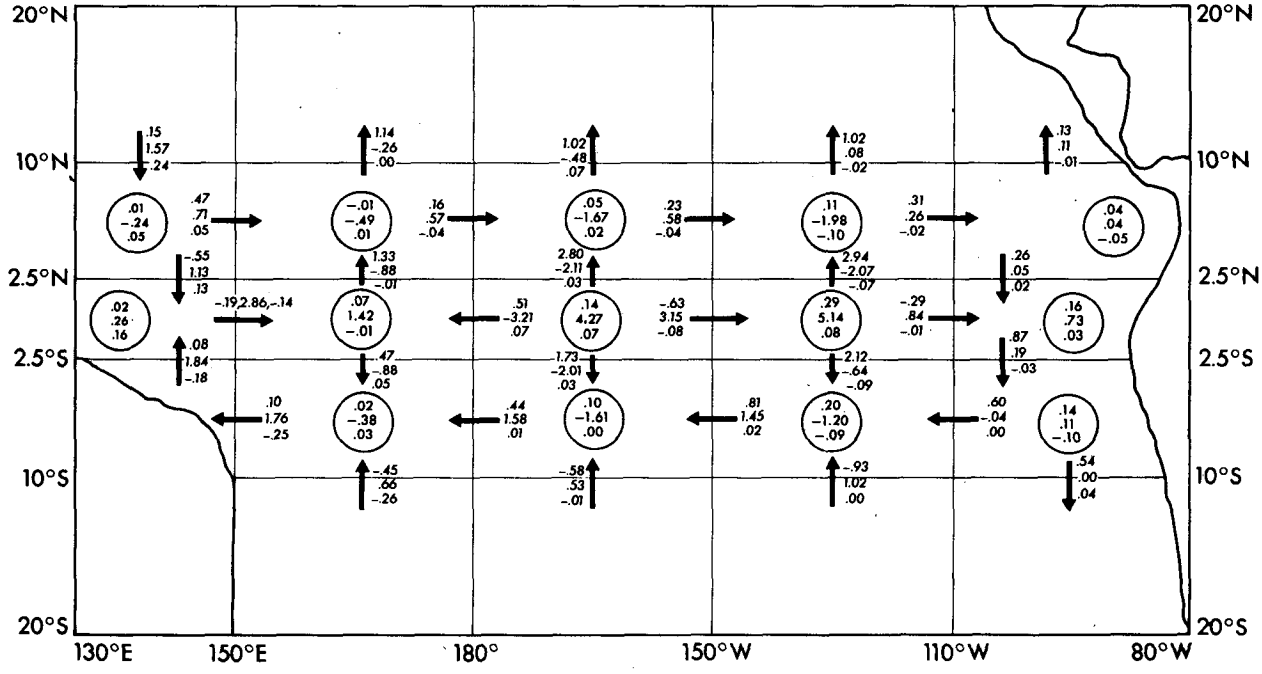

FIG. 17. The annual mean heat budget of different boxes into which the model has been divided. The upper number in the circles is the annual mean heat flux across the ocean surface; the lower numbers are the heat fluxes across horizontal surfaces at 50 and 317 m, respectively (positive if upward). A triad of numbers indicates the horizontal heat flux across the indicated vertical surface in the upper 50 m, between 50 and 317 m and below 317 m. A negative sign means the flux is opposite to the ocean. All units are 10^{15} W.

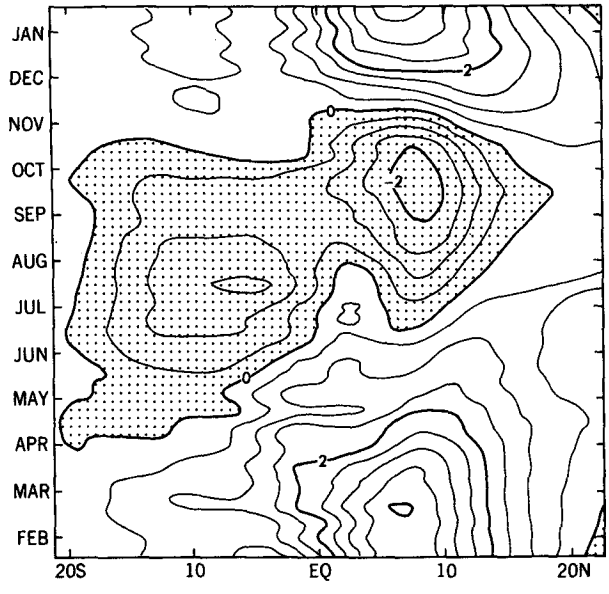

FIG. 18. The zonally integrated meridional heat transport (in units of 10^{15} W). The transport is southward in shaded areas.

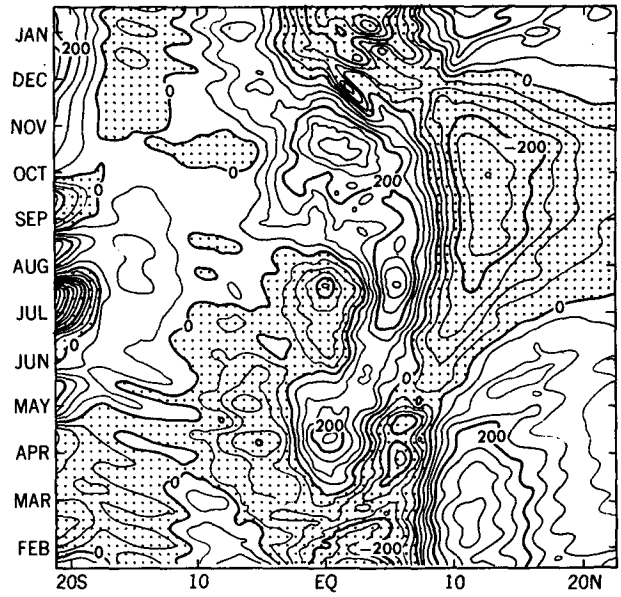

FIG. 20. The rate of change of the zonally integrated heat storage (which is the vertical integral, from the ocean floor to the surface, of the temperature). The contour interval is 0.5×10^7 W m^{-1}.

The water from the latter current wells up along the equator and is heated by the flux across the surface while it flows westward and sinks near 3°N.

7. Discussion

Descriptions of the mass and heat budgets of the ocean necessarily rely on dynamical models to compensate for the unavailability of certain measurements. This paper uses the most sophisticated model available, a general circulation model which simulates the tropical oceans realistically, provided accurate surface winds force the model. This proviso precludes a detailed comparison between the results presented here and measurements in the tropical Pacific Ocean. Because of the considerable interannual variability in the Pacific, the winds in a given year are unlikely to correspond to the climatological conditions that force the model. Hence, oceanic measurements over a prolonged period are needed for comparison with the response of a model forced with climatological winds. Data for this purpose are very sparse, but they confirm the salient features of the seasonal cycle in the model. Wyrtki (1974) describes large changes in the intensity of the North Equatorial Countercurrent which is intense in the Northern Hemisphere autumn and is weak in the spring. Levitus (1984) uses historical hydrographic data to document that seasonal variations in the oceanic heat storage are 180° out of phase across approximately 9°N. Halpern (1987), Hayes and Halpern (1984) and Lukas (1986) describe an eastward surge of warm water along the equator in the spring when the southeast trades relax. Both the amplitude and the phase of the seasonal changes in the intensity of the Equatorial Undercurrent are realistic. Considerable amounts of data have been collected over the past few years, and continue to be collected, so that a stringent test for the model will soon be possible, provided it is forced with the winds that prevailed during the time of the measurements. But first, it will be necessary to remedy some of the flaws in the model: the absence of islands and realistic bottom topography and the idealized geometry

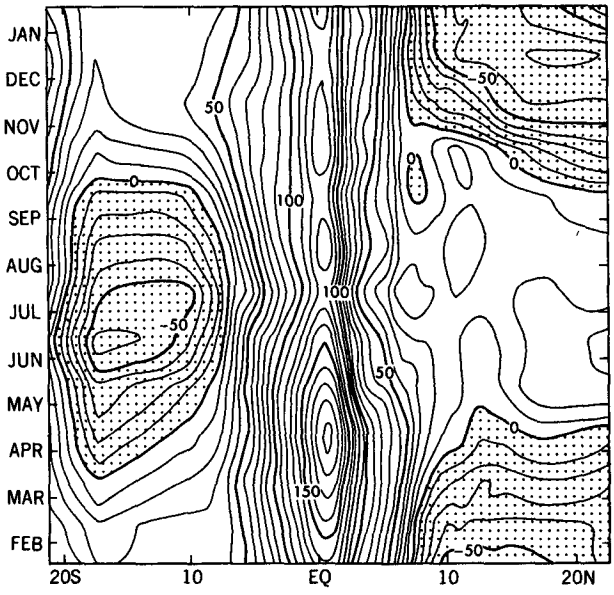

FIG. 19. The zonally integrated heat flux (in units of 10^5 W m^{-1}, upward out of the ocean in shaded regions).

of the western side of the ocean basin, for example. (Measurements to determine mass and heat transport into the Indian Ocean, and to determine variations in the southward-flowing boundary current along the eastern coast of the Philippines will be of considerable interest because, in the model, the heat transport associated with that flow is very important in the seasonal heat budget.) The parameterization of mixing processes in the model needs to be improved because the observed mixed surface layer, which extends to approximately 150 m in the western equatorial Pacific, and which is bounded below by a very sharp thermocline, appears in the model as a weakly stratified layer bounded below by a rather diffuse thermocline. The inadequate mixing may be related to the specification of monthly mean winds to force the model because, in reality, the high-frequency wind fluctuations may contribute to considerable mixing. Inadequate mixing in the thermostad below the equatorial thermocline may also be part of the reason why the deep eastward countercurrents observed at the northern and southern edges of the thermostad are absent from the model. These matters are currently being investigated.

Measurements with which to calculate the mass and heat budgets of the tropical Pacific Ocean are unavailable and are likely to be so for a considerable time. It is therefore necessary to use the very limited and inadequate available data together with dynamical models to study the mass and heat budgets. In our calculations, the historical hydrographic data were used as initial conditions and a general circulation model was used to calculate the modified temperature field, and the associated currents that are consistent with the specified winds. Improved estimates of the heat and mass budgets will be possible once the model uses the available data not merely as initial conditions, but as constraints during its integration in time. Methods for the assimilation of data into models, thus resulting in an overspecified system, are currently being developed.

Acknowledgments. This paper is dedicated to the memory of Dr. Adrian Gill, whose keen and active interest in tropical oceanography stimulated us all. We are indebted to Ms. W. Marshall and Mr. P. Tunison and his staff for assistance in the preparation of this paper.

REFERENCES

Bryan, K., 1969: A numerical method for the study of the world ocean. *J. Comput. Phys.*, **4**, 347–376.

——, 1982: Poleward heat transport in the oceans: Observations and models. *Ann. Rev. Earth Planet. Sci.*, **10**, 15–38.

Bryden, H., and E. C. Brady, 1985: Diagnostic model of the three-dimensional circulation of the upper equatorial Pacific Ocean. *J. Phys. Oceanogr.*, **15**, 1255–1273.

Busalacchi, A. J., and J. J. O'Brien, 1980: The seasonal variability in a model of the tropical Pacific. *J. Phys. Oceanogr.*, **10**, 1929–1951.

Cane, M. A., 1979: The response of an equatorial ocean to simple windstress patterns. *J. Mar. Res.*, **37**, 253–299.

——, and D. W. Moore, 1981: A note on low frequency equatorial basin modes. *J. Phys. Oceanogr.*, **11**, 1578–1584.

Enfield, D. B., 1986: Zonal and seasonal variability of the equatorial Pacific heat balance. *J. Phys. Oceanogr.*, **16**, 1038–1054.

Garzoli, S., and S. G. H. Philander, 1985: Validation of an equatorial Atlantic model using inverted echo sounder data. *J. Geophys. Res.*, **90**, 9199–9201.

Halpern, D., 1987: Observations of annual and interannual thermal and flow variations along the equator in the eastern Pacific Ocean during 1980–1985. *J. Geophys. Res.*, (in press).

Hasunuma, K., and K. Yoshida, 1978: Splitting of the subtropical gyre in the western north Pacific. *J. Oceanogr. Soc. Japan*, **34**, 170–172.

Hayes, S. P., and D. Halpern, 1984: Correlation of upper ocean currents and sea level in the eastern equatorial Pacific. *J. Phys. Oceanogr.*, **14**, 811–824.

——, J. M. Toole and L. J. Mangum, 1983: Water mass and transport variability at 110°W in the equatorial Pacific. *J. Phys. Oceanogr.*, **13**, 153–168.

Hellerman, S., and M. Rosenstein, 1983: Normal monthly windstress over the world ocean with error estimates. *J. Phys. Oceanogr.*, **13**, 1093–1104.

Hisard, P., J. Merle and B. Voituriez, 1970: The Equatorial Undercurrent at 170°E in March and April 1967. *J. Mar. Res.*, **28**, 281–303.

Levitus, S., 1982: *Climatological Atlas of the World Ocean.* NOAA Prof. Paper 13, 173 pp., 17 microfiche, U.S. Govt. Printing Office, Washington, D.C.

——, 1984: Annual cycle of temperature and heat storage in the world ocean. *J. Phys. Oceanogr.*, **14**, 727–746.

Lukas, R., 1986: The termination of the Equatorial Undercurrent in the eastern Pacific. *Progress in Oceanography*, Vol. 16, Pergamon, 63–90.

Meyers, G., 1979: Annual variation of the slope of the 14°C isotherm along the equator in the Pacific Ocean. *J. Phys. Oceanogr.*, **9**, 885–891.

Pacanowski, R., and S. G. H. Philander, 1981: Parameterization of vertical mixing in numerical models of tropical oceans. *J. Phys. Oceanogr.*, **11**, 1443–1451.

Pares-Sierra, A. F., M. Inoue and J. J. O'Brien, 1985: Estimates of oceanic heat transport in the tropical Pacific. *J. Geophys. Res.*, **90**, 3293–3303.

Philander, S. G. H., and W. J. Hurlin, 1987: Initial conditions for General Circulation Models of tropical oceans. *J. Phys. Oceanogr.*, **17**, 147–157.

——, and R. C. Pacanowski, 1980: The generation of equatorial currents. *J. Geophys. Res.*, **85**, 1123–1136.

——, and ——, 1986: A model of the seasonal cycle in the tropical Atlantic Ocean. *J. Geophys. Res.*, **91**, 14 192–14 206.

——, and A. D. Seigel, 1985: Simulation of El Niño of 1982–1983. *Coupled Ocean-Atmosphere Models.* J. Nihoul, Ed., Elsevier, 517–541.

——, W. J. Hurlin and R. C. Pacanowski, 1986: Properties of long equatorial waves in models of the seasonal cycle in the tropical Atlantic and Pacific Oceans. *J. Geophys. Res.*, **91**, 14 207–14 211.

Richardson, P. L., and S. G. H. Philander, 1987: The seasonal variations of surface currents in the tropical Atlantic Ocean. *J. Geophys. Res.*, **34**, 123–137.

Taft, B. A., 1967: Equatorial undercurrent in the Indian Ocean. *Studies in Tropical Oceanography*, **5**, 3–14, University of Miami Press.

Wyrtki, K., 1974: Sea level and seasonal fluctuations of the equatorial currents in the western Pacific Ocean. *J. Phys. Oceanogr.*, **4**, 91–103.

——, 1981: An estimate of equatorial upwelling in the Pacific. *J. Phys. Oceanogr.*, **11**, 1205–1214.